DOI: 10.61782/fa.2025.0410

FORUM ACUSTICUM EURONOISE 2025

FRAMEWORK FOR THE ASSESSMENT OF UNCERTAINTY OF HIGH-SPEED TRAIN PANTOGRAPH AERODYNAMIC NOISE PREDICTIONS

Eduardo Latorre Iglesias[1*] **Guillermo García Barrios**[2] **María Luisa López Ibáñez**[1]
Aurora Melis[1] **Jorge Muñoz Paniagua**[3] **David Thompson**[4]
[1] Grupo de Acústica Arquitectónica, E. T. S. de Arquitectura, Universidad Politécnica de Madrid, Spain
[2] 5G Communications for Future Industry Verticals S.L. (Fivecomm), Camí de Vera s/n (6D building), 46022 Valencia, Spain
[3] E.T.S. de Ingenieros Industriales, Universidad Politécnica de Madrid, Spain
[4] Institute of Sound and Vibration Research, University of Southampton, United Kingdom

ABSTRACT

Noise predictions are normally used to evaluate compliance with regulations, to validate the design of new trains or for virtual certification in cases where existing trains are modified. Hence, prediction uncertainty should be considered to minimize risks. Although for measurements, a methodology for the assessment of uncertainty is well defined in the Guide for Uncertainty in Measurements (GUM), there is a lack of standardised procedures for predictions. This work proposes a framework for uncertainty assessment of aerodynamic noise predictions for a high-speed train pantograph using a component-based model. A sensitivity analysis is applied to select the relevant input parameters; uncertainty propagation is calculated assuming a Gaussian distribution and using the law of propagation of uncertainty for measurements given in the GUM. An example of the application of the proposed framework is given for pass-by noise predictions of a generic high-speed train pantograph installed in a train running at 330 km/h. The results show the feasibility of applying the proposed framework for uncertainty assessment of this specific case, but also the potential for application to railway exterior noise predictions using different prediction models.

Keywords: *railway noise, prediction, uncertainty, high-speed train, pantograph.*

[*] ***Corresponding author***: *eduardo.latorre.iglesias@upm.es.*

1. INTRODUCTION

Aerodynamic noise becomes significant when high-speed trains run at speeds above around 300 km/h [1]. During train pass-by at these speeds, the maximum noise level is normally associated with the pantograph, which produces a significant peak in the noise time history [2]. Its contribution to the average noise during pass-by could also be important [3]. As the pantograph is installed on the train roof above the top edge of noise barriers, their efficiency decreases due to a reduction of sound screening [4]. Although broadband noise is also produced, the aerodynamic noise produced by pantographs is mainly tonal, and it is generated by vortex shedding due to the interaction of the incoming airflow with the pantograph components.

In recent years different prediction methods have been applied to estimate the aerodynamic noise generated by high-speed pantographs. Accurate predictions can be made using numerical models based on Computer Fluid Dynamics (CFD) and Computational AeroAcoustics (CAA). Although these calculations are demanding in terms of high computational time and cost, they are currently widely used [5, 6]. An alternative is to use component-based semi-empirical models [7,8], which allow for quick predictions of the pantograph aerodynamic noise and provide the contribution to the overall noise of pantograph components. This makes them useful to estimate the impact on the radiated noise when geometrical modifications are made and to propose noise mitigation strategies within the framework of a real project, normally with tight deadlines.

Lately, the railway industry shows interest in developing a framework for virtual train certification to save time and cost

with respect to the current procedure that involves field tests [9, 10]. To this aim, robust prediction tools that include uncertainty assessment of the results shall be developed. Bognini et al. presented guidance for estimating the uncertainties of the exterior train noise calculations made with different calculation tools normally used by train manufacturers and operators [11]. Similarly, a framework for uncertainty assessment for the train noise prediction tool SITARE was developed in [12]. This is based on the methodology proposed in the Guide for Uncertainty in Measurements (GUM) [13] for the assessment of the uncertainty in measurements from the propagation of the input uncertainties. It is applied to obtain the uncertainty of the predicted pass-by noise of a complete train based on the uncertainty of the model inputs: sound power level and directivity of each individual noise source and train geometry. An application of the proposed framework for uncertainty assessment to real cases can be found in [14].

In this work a framework is presented for the calculation of the uncertainty in the high-speed train pantograph aerodynamic noise obtained using the component-based model presented in [7]. The motivation for this work is to provide a robust uncertainty assessment method to be applied to the component-based model to make it adequate for virtual train certification. In Section 2, a sensitivity analysis is applied to select the relevant input parameters. In Section 3, uncertainty propagation is calculated assuming a Gaussian distribution and using the law of propagation of uncertainty for measurements given in the GUM. Section 4 includes a Monte-Carlo method used to evaluate the validity of the previous assumptions. Finally, an example of the application of the proposed framework is given in Section 5 for pass-by noise predictions of a generic high-speed train pantograph installed in a train running at 330 km/h.

2. COMPONENT-BASED MODEL AND FRAMEWORK FOR UNCERTAINTY ASSESSMENT

The semi-empirical component-based prediction model is based on the assumption that the overall mean square sound pressure radiated by the train pantograph exposed to an incoming flow can be expressed as the incoherent sum of the spectra of each individual components, as follows [7]:

$$\overline{p^2}(x) = \frac{\rho_0^2}{16 c_0^2} \sum_i \frac{U_i^6 S_i \eta_i D_{rad_i}(\psi, \phi)}{R_i^2} \qquad (1)$$

where ρ_0 is the air density, c_0 is the speed of sound, U_i is the incident flow speed, R_i is the distance between the component and the receiver, η_i is the amplitude factor, S_i is the total surface area of the component, and the subscript i refers to each component. The directivity function $D_{\mathrm{rad},i}(\psi, \phi)$ is dependent on the angles, ψ, ϕ, Fig. 1 shows the definition of the angles ψ, ϕ, with respect to the centre of a cylinder representing a pantograph component.

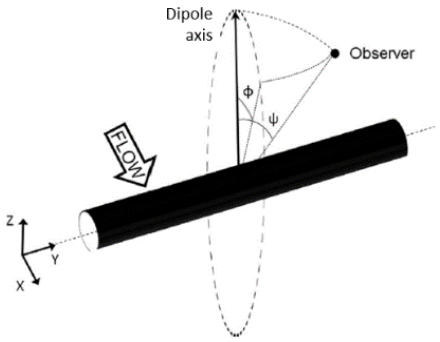

Figure 1. Sketch showing the definition of angles ψ and ϕ for a cylinder representing a pantograph component and considering the air flow direction.

The amplitude factor η_i for each component i is chosen to fit the predicted noise to a reference spectrum. For simplicity, the convective amplification effect is neglected. The normalized spectrum, obtained in the reference prediction model by fitting the shape of a given function to that of the reference measurement, is here omitted as only the overall noise level is considered.

The noise radiated by each pantograph component can be expressed in terms of Sound Pressure Level (SPL) as follows:

$$L_{p,i} = 10\log_{10}\left(\frac{\overline{p_i^2}(x)}{p_{\mathrm{ref}}^2}\right) \qquad (2)$$

where $\overline{p_i^2}(x)$ is the mean square sound pressure spectrum radiated by each pantograph component, and $p_{\mathrm{ref}} = 2 \times 10^{-5}$ Pa. Hence, the overall SPL radiated by the pantograph can be obtained as the energetic sum of the SPL of each component as follows:

$$L_{p,t} = 10\log_{10}\left(\sum_{i=1}^{N} 10^{L_{p,i}/10}\right) \qquad (3)$$

According to the GUM, when carrying out experiments the measurand Y is normally an estimation of the measurement with an associated uncertainty, y. In many cases, this is not directly measured but estimated from several input quantities X with a functional relationship among them, f, where the input quantities will have an associated uncertainty. In this case this functional relation is given by Eq. (1). It can be

inferred that the uncertainty of the result, $u(y)$, depends on the uncertainties of the input quantities, $u(x)$. If the input quantities are statistically uncorrelated, this relation is given by

$$u_c^2(y) = \sum_{j=1}^{K} \left(\frac{\partial f}{\partial x_j}\right)^2 u^2(x_j) \quad (4)$$

or if they are totally correlated by

$$u_c(y) = \sum_{j=1}^{K} \left(\frac{\partial f}{\partial x_i}\right) u(x_j) \quad (5)$$

where K is the number of input parameters [13]. For simplicity, statistical partial correlation between input uncertainties is not considered. The functional relation between the overall pantograph noise level and the noise level produced by each individual component is as follows (assuming that its uncertainties are correlated, as the noise is added incoherently):

$$u(L_{p,t}) = \sum_{i=1}^{N} c_i\, u(L_{p,i}) \quad (6)$$

where the sensitivity factor, $c_{L_{p,i}}$, is given by:

$$c_{L_{p,i}} = {}^{\partial L_{p,t}}\!/_{\partial L_{p,i}} = \frac{10^{{}^{L_{pi}}/_{10}}}{\sum_{i=1}^{N} 10^{{}^{L_{pi}}/_{10}}} \quad (7)$$

and

$$u(L_{p,i}) = \left(\frac{\partial L_{p,i}}{\partial \overline{p_i^2}(x)}\right) u\left(\overline{p_i^2}(x)\right) \quad (8)$$

The uncertainty of the estimated mean square sound pressure, $u(\overline{p_i^2}(x))$, can be expressed in terms of the uncertainties of the input quantities given in Eq. (1), namely the uncertainty of the incident flow speed, $u(U_i)$, amplitude factor, $u(\eta_i)$, surface area, $u(S_i)$, directivity factor, $u(D_i)$, and distance from the source to the receiver, $u(R_i)$, and the related sensitivity coefficients as follows

$$u^2\left(\overline{p_i^2}(x)\right) = c_{U,i}^2 u^2(U_i) + c_{\eta,i}^2 u^2(\eta_i) + c_{S,i}^2 u^2(S_i) + c_{R,i}^2 u^2(R_i) + c_{D,i}^2 u^2\left(D_{rad_i}\right) \quad (9)$$

where the sensitivity factors, c, represent the partial derivative of the averaged squared sound pressure obtained using Eq. (1) by each of the different input parameters.

3. INPUT UNCERTAINTIES

3.1 Sensitivity analysis

When possible, input uncertainties are estimated as 'type A' from measured data, based on the assumption that the best available estimate of the input parameter is the averaged value of *n* independent observations, and the best estimate of its uncertainty is the standard deviation of the mean. In some cases, there is a lack of experimental data, so the uncertainty of the model input quantities is approximated following a scientific judgment ('type B' uncertainties).

For instance, the geometrical parameters of the pantograph components (i.e., length, diameter, cross-section) are obtained from CAD software, with high precision. Hence, the uncertainty of the component surface area is assumed to be small (~ 1 mm^2). The uncertainty in the distance between the microphone position and the geometrical centre of each pantograph component can also be defined with high accuracy in the predictions. If the acoustic centre is considered instead, it seems more complicated to define this distance accurately, as the vortex shedding process occurs along the whole component length with a certain correlation. To simplify things, in the prediction model it is assumed the acoustic centre coincides with the geometrical centre of the component; considering this assumption the uncertainty in distance between source and receiver is supposed to be small (~ 1 cm).

It is assumed that the noise produced by each of the pantograph struts is governed by vortex shedding. A simple approach is to model this type of noise source using the directivity of a theoretical dipole. This assumption was shown to be reasonable with deviations between measurements carried out in anechoic chamber and the theoretical results of less than 3 dB for angles between -50º and 70º [15]. For an angle of 90º a noise reduction up to 20 dB is obtained in the experiments, while for a theoretical dipole no noise would be radiated. In the component-based prediction model, the maximum difference between the noise radiated in the dipole radiation axis (0º) and for angles larger than 70º is therefore limited to -20 dB. The directivity of a theoretical dipole can be expressed as:

$$D_{rad_i}(\psi, \phi) = \cos(\psi)\cos(\phi) \quad (10)$$

Assuming that the uncertainties of both angles, $u(\psi)$ and $u(\phi)$, are statistically uncorrelated, the uncertainty of the directivity factor can be defined as:

$$u\left(D_{rad_i}(\psi, \phi)\right) = \sqrt{c_\psi^2 u^2(\psi) + c_\phi^2 u^2(\phi)} \quad (11)$$

Fig. 2 shows the relative position of the microphone with respect to the pantograph head. During the anechoic wind tunnel test used in [7] to validate the component-based model, the microphone was placed perpendicular to the current collector, at 5 m from its centre (i.e., for $\beta = 0°$ and $\gamma = 0°$ according to Fig. 2).

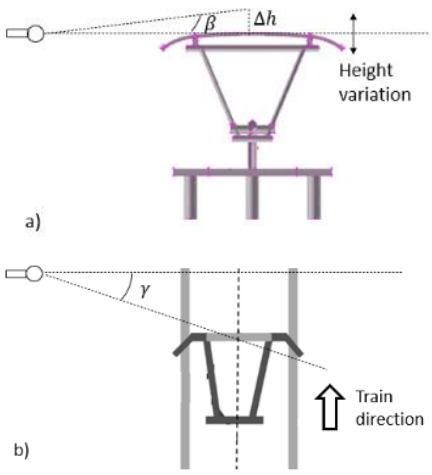

Figure 2. Sketch showing the definition of the angles β and γ taken as reference the centre of the current collector.

For a stationary pantograph, as is the case during the wind tunnel tests, the angle γ between the microphone axis and the dipole radiation axis for each pantograph bar does not vary with time and can be assessed accurately, so it seems reasonable to neglect its uncertainty, $u(\gamma)$. If a calculation is made to assess the average noise during train pass-by, the angle γ has to be estimated for different positions of the pantograph along the rail, leading to different relative positions between each pantograph component radiation axis and the microphone position. In this case, this angle will be more difficult to assess accurately, and its uncertainty should be considered. In the case considered here it can be assumed that $\psi \approx 0$, and hence $D_{\mathrm{rad}_i}(\psi,\phi) \sim \cos(\phi)$.

The height, h, is defined as the height of the centre of the pantograph with respect to the ground. Variations in the height of the pantograph head, Δh, can lead to variations in the angle β "seen" by the microphone, especially regarding horizontal bars such as the current collector. Therefore, the variations of the angle ϕ between the dipole radiation axis and the microphone axis can be expressed in terms of the variation of the pantograph height during operation as $\phi = \phi_0 + \beta$, and β can be expressed as function of the height variation, Δh, and distance, d, as $\beta = \cos^{-1}(\Delta h/d)$, hence

$$u^2(D_{rad}) \sim u^2(\phi) = c_{\Delta h}^2 u^2(\Delta h) + c_d^2 u^2(d) \quad (12)$$

$$c_{\Delta h} = \left(-d\sqrt{1 - {(\Delta h)^2}/{d^2}}\right)^{-1} \quad (13)$$

$$c_d = \left(\frac{d^2}{h}\sqrt{1 - {(\Delta h)^2}/{d^2}}\right)^{-1} \quad (14)$$

Variation in the height of the pantograph head can occur due to arching of the contact wire between fixing points. The pantograph adjusts its height to guarantee the contact between collector and catenary and to maintain the contact force as constant as possible. To estimate the pantograph height variations for high-speed trains, three experimental studies are used. Song et. al [16] have obtained the heights of the key points in the contact wire of a Chinese high-speed train track using a device that consisted of a laser and a camera installed in an inspection vehicle. Their statistical distribution is described by the power spectrum density (PSD) function. Usuda and Ikeda presented static contact wire height measured in a high-speed track using a train running at 270 km/h [17]. Koyama et al. have measured the variation of the pantograph head in a commercial Shinkansen train running with maximum speed of 300 km/h. Two-line sensor cameras and lighting were mounted near the pantograph. By tracking the movement of three markers placed on different surfaces of the pantograph head, the displacement was obtained [18]. Fig. 3 shows a histogram that represents the pantograph head variation obtained in the three experimental works cited above.

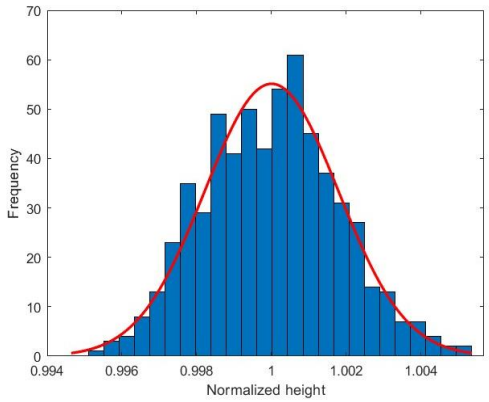

Figure 3. Histogram of the normalised pantograph height obtained for a high-speed train running in normal conditions in [16-18].

The obtained histogram is compared with that expected for a Gaussian distribution, giving reasonable agreement. The pantograph height has been normalized using the measured mean value (5.3 m). The results are fitted to a standard normal distribution. The uncertainty in the estimation of the pantograph contract strip height, $u(\Delta h)$, can be expressed as the standard deviation of the mean considering a standard deviation $\sigma = 0.0018$ and $n = 602$ samples, giving $u(\Delta h) = 0.4$ mm and an expanded uncertainty for $k = 2$ of $U(\Delta h) = 0.8$ mm.

The amplitude factor in Eq. (1), η_i, for a specific component *i*, is obtained in the component-based model as follows:

$$\eta = St^2 C_{Lrms}^2 l_c L D \tag{15}$$

where D is the component characteristic dimension, St is the Strouhal number, C_{Lrms}^2 is the root mean square (rms) fluctuating lift coefficient, l_c is the spanwise correlation length normalized by D, and L is the component length. An initial value of the amplitude factor, $\eta_{0,i}$, is defined for the reference cases comprising a circular cylinder and a square bar. The reference values of St, C_{Lrms}^2 and l_c needed to estimate η_0 are approximated from results found in the literature [19]. Assuming uncorrelated input uncertainties, the uncertainty in the calculation of the initial value of the amplitude factor, can be obtained from

$$u^2(\eta_0) = c_{\eta_0}^2 u^2(St) + c_{C_{Lrms}}^2 u^2(C_{Lrms}) + c_{l_c}^2 u^2(l_c) + c_D^2 u^2(D) + c_L^2 u^2(L) \tag{16}$$

where $u(St)$ is the uncertainty of the obtained Strouhal number, $u(C_{Lrms})$ is the uncertainty of the rms fluctuating lift coefficient, and $u(l_c)$ is the uncertainty in the spanwise correlation length. These uncertainties are estimated as the standard deviation of the mean obtained with the available data. The sensitivity factors in Eq. (16) are obtained as follows:

$$c_{St} = \partial\eta_0/\partial St = 2St C_{L,rms}^2 l_c L D \tag{17}$$

$$c_{C_{Lrms}} = \partial\eta_0/\partial C_{Lrms} = 2St^2 C_{Lrms} l_c L D \tag{18}$$

$$c_{l_c} = \partial\eta_0/\partial l_c = St^2 C_{L,rms}^2 L D \tag{19}$$

$$c_L = \partial\eta_0/\partial L = St^2 C_{L,rms}^2 l_c D \tag{20}$$

$$c_D = \partial\eta_0/\partial D = St^2 C_{L,rms}^2 l_c L \tag{21}$$

A significant number of experimental and numerical investigations are found in the literature on aerodynamic parameters related to vortex shedding from circular cylinders, such as rms fluctuating lift coefficient, correlation length and Strouhal number. An extensive review is provided by Norberg [19] comparing the variation of the above-mentioned parameters for a broad range of Reynolds numbers within the subcritical regime ($1.0 \times 10^4 \leq Re \leq 1.0 \times 10^5$). Results ignore end effects (cylinder aspect ratio > 25). Fig. 4 shows the values of the different parameters obtained from [19]. A constant value of each of them is expected in the subcritical regime. A continuous line shows the mean values, while dotted lines show a range of +/- one standard deviation. In this work, this analysis is only carried out for circular cylinders. It is planned to extend the analysis to bars with different cross-sections in future work.

Tab. 1 shows the mean value, μ, standard deviation, σ, uncertainty, u, sensitivity coefficient, c and contribution to the uncertainty of the reference value of the amplitude factor, $u(\eta_0)$, of each of the relevant parameters. In the case of the geometrical parameters D and L, a reasonable value of the uncertainty is chosen based on experience.

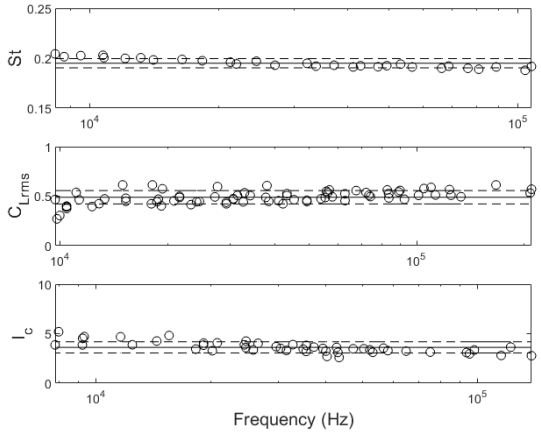

Figure 4. Values of Strouhal number, St, rms fluctuating lift coefficient C_{Lrms}^2 and correlation length l_c obtained from [19]. (−) Mean value. (--) Mean value +/- standard deviation.

Table 1. Mean value, μ, standard deviation, σ, number of independent observations, n, uncertainty, u, and sensitivity factor, c used for the parameters needed to calculate η_0.

	St	C_{Lrms}^2	l_c	D	L
μ	0.19	0.49	3.62	0.05	1.25
σ	0.038	0.067	0.564	-	-
n	37	74	47	-	-
u	$0.8\ 10^{-3}$	$7.8\ 10^{-3}$	0.08	1%	1%
c	0.02	$8.4\ 10^{-3}$	$0.6\ 10^{-3}$	0.41	$1.6\ 10^{-3}$
$(cu)^2$	$0.3\ 10^{-9}$	$4.3\ 10^{-9}$	$2.2\ 10^{-9}$	$0.4\ 10^{-9}$	$0.4\ 10^{-9}$

Regarding the uncertainty in the incoming flow speed, Tab. 2 gives the mean and standard deviation (between brackets) of the incident flow speed of the pantograph head from [8], based on published measurements, for full and reduced scale of a variety of train types with no cross wind. Results are included for two different pantograph types (1 and 2) in two different configurations (pantograph knee pointing upstream and downstream, depending on the train running direction).

These were measured at different distances from the front of the train and for a range of pantograph head heights above the train roof.

Table 2. Incident flow speed for the panhead for different pantograph types and configurations [8].

Panto graph	Knee	Distance (m)	Height (m)	U (m/s)
1	Downstream	280	0.7-0.8	0.84 (0.03)
1	Upstream	100	0.7-0.8	0.88 (0.03)
2	Downstream	100	1.0-1.2	0.90 (0.03)
2	Upstream	40	1.0-1.2	0.93 (0.03)

The sensitivity coefficients obtained from the derivative of Eq. (1) and Eq. (2) by each of the input quantities:

$$\frac{\partial L_p}{\partial U} = \frac{\partial L_p}{\partial \overline{p^2}(x)} \frac{\partial \overline{p^2}(x)}{\partial U} = c_{L_p} c_U = \frac{60}{\mathrm{Ln}(10) U} \tag{22}$$

$$\frac{\partial L_p}{\partial \eta} = \frac{\partial L_{pi}}{\partial \overline{p^2}(x)} \frac{\partial \overline{p^2}(x)}{\partial \eta} = c_{L_p} c_\eta = \frac{10}{\mathrm{Ln}(10) \eta} \tag{23}$$

$$\frac{\partial L_p}{\partial S} = \frac{\partial L_{pi}}{\partial \overline{p^2}(x)} \frac{\partial \overline{p^2}(x)}{\partial S} = c_{L_p} c_S = \frac{10}{\mathrm{Ln}(10) S} \tag{24}$$

$$\frac{\partial L_p}{\partial R} = \frac{\partial L_{pi}}{\partial \overline{p^2}(x)} \frac{\partial \overline{p^2}(x)}{\partial R} = c_{L_p} c_R = \frac{-20}{\mathrm{Ln}(10) R} \tag{25}$$

$$\frac{\partial L_p}{\partial D_{\mathrm{rad}}} = \frac{\partial L_{pi}}{\partial \overline{p^2}(x)} \frac{\partial \overline{p^2}(x)}{\partial D_{\mathrm{rad}}} = c_{L_p} c_{D_{\mathrm{rad}}} = \frac{10}{\mathrm{Ln}(10) D_{rad}} \tag{26}$$

4. UNCERTAINTY OF THE RESULTS

A pantograph is composed of many struts. Fig. 5 shows a sketch of a DSA350 pantograph, identifying the struts considered in the prediction model. To reduce the calculation time (especially when running Monte Carlo simulations), only the relevant components are chosen for the uncertainty calculations. To do so, the contribution of each component to the overall noise radiated by the pantograph is assessed by comparing their sensitivity factors calculated by means of Eq. (7). Tab. 3 shows the selected components considering sensitivity factors above 0.03, which represents a 3% contribution to the overall squared pressure. The overall noise obtained in the predictions considering all the pantograph components is 103.2 dB, while 102.0 dB is obtained considering only the components shown in Tab. 1.

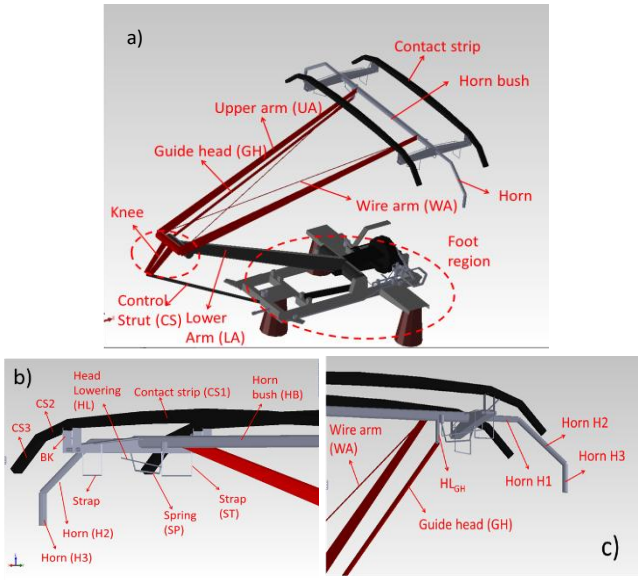

Figure 5. Pantograph DSA350 and main components.

Table 3. Contribution to the overall pantograph noise due to the selected pantograph components.

Component	L_{p_i}, dB	$c_{L_{p,i}}$
Upstream contact strip (uCS1)	99.9	0.469
Guide Head (GH)	92.6	0.086
Head lowering (HL)	90.7	0.057
Horn bush (HB)	89.1	0.039
Downstream contact strip (dCS1)	88.6	0.035
Upstream strap close (uSTc)	88.5	0.034
Upstream strap far (uSTf)	88.5	0.034
Overall, L_{p_t}	102.0	

In this study, for the uncertainty calculation all the components are assumed to be circular cylinders (it is not the case for the actual noise level calculations), and the same uncertainty due to directivity is taken for all components, independently of their position relative to the microphone. This yields the same uncertainty for the predicted noise of all components. Tab. 4 shows the sensitivity coefficients, uncertainty and contribution to the overall uncertainty for the different input parameters. According to the results presented in Tab. 4, the two parameters with the largest contribution to the uncertainty of the predicted pantograph noise are the incident flow speed, U, and the amplitude factor, η.

Table 4. Sensitivity coefficient, c, uncertainty, u, and contribution to the overall uncertainty for the different input parameters.

Parameter	c	u	$(cu)^2$
U	0.29	1.65	0.2340
η_i	25.1	$4.9\ 10^{-5}$	0.0006
S	8087.4	0.001	0.1630
R_i	-1.73	0.01	0.0003
D_{rad}	-16.2	$1.6\ 10^{-3}$	0.0007

Substituting values from Tab. 4 in Eq.(16) gives the uncertainty of the sound pressure level due to the complete pantograph $u(L_{p,t})$ = 0.6 dB (note that, due to the specific case considered here, this uncertainty is the same as that of an individual component, i.e. $u(L_{p,t}) = u(L_{p,i})$), and an extended uncertainty for k = 2 of $U(L_{p,i})$ = 1.2 dB. The difference found between predictions and wind tunnel tests in [7] using the same pantograph for a flow speed of 330 km/h is -0.7 dB(A), so the uncertainty obtained seems to be reasonable.

The applied uncertainty propagation method assumes a Gaussian distribution of the uncertainty of the predicted results. This might not be the case, so Monte Carlo simulations should be carried out to validate this hypothesis. In addition, the uncertainty obtained is probably underestimated. In this study, only the propagation of the input uncertainties is considered; the uncertainty due to the model itself is not considered. This is relevant for pantograph components which are not the reference case considered here (non-inclined circular cylinder), because in the component-based model the values of the empirical constants adjusted for the reference case are modified to account for the effect of different factors: inclination angle, different cross-sectional shapes, short aspect ratio that leads to end effects, incoming turbulence intensity, etc. Most of these adjustments are based on curve fitting from a limited dataset, so an inherent error is assumed.

5. LIMITATIONS OF THE CURRENT FRAMEWORK AND FUTURE WORK

The limitations in the application of the current framework due to simplifications made in this work can be summarized:

- Predictive uncertainties describing the variability of the predictions with respect to the real case due to the model assumptions and simplifications are not considered.
- All the pantograph components are assumed to be non-inclined circular cylinders (reference case). This avoids modification of the values of the empirical constants that will increase the uncertainty of the result.
- The effect of modelling the vortex shedding noise produced by pantograph struts as a theoretical dipole placed at the geometrical centre of the strut is not considered.
- The uncertainty of the amplitude factor is approximated using data for circular cylinders only.
- A Gaussian distribution of the prediction uncertainty is assumed.

Despite carrying out actions to address the limitations mentioned above, as future work it is planned to perform Monte Carlo simulations to verify the validity of the assumption of a Gaussian distribution of the prediction uncertainty. The uncertainty of each individual component will be obtained considering their particular geometry, inclination angle and incident flow speed and turbulent intensity. Moreover, a calculation of the uncertainty of train pass-by noise will be of major interest.

6. CONCLUSIONS

A framework for the assessment of the uncertainty in the aerodynamic noise of a high-speed train predicted using a component-based model is presented. This is based on the propagation of the uncertainty of the model inputs assuming a Gaussian distribution. The input parameters considered are the incident flow speed, the model amplitude factor, distance between the pantograph head centre and the microphone, pantograph component surface area and source directivity. The sensitivity factors of each of the input parameters are obtained from the derivatives of the prediction model equations. The input uncertainties are estimated as standard deviations of the mean when experimental data are available, or by scientific judgment or experience when data is scarce. An expanded uncertainty (k = 2) of 1.2 dB in the overall predicted sound pressure level radiated by a high-speed pantograph is obtained, for a flow speed of 330 km/h and a microphone at 5 m from the pantograph head centre. The input parameters that contribute the most to the uncertainty of the results are the incoming flow speed and the amplitude factor. The results obtained show the potential of the proposed framework to be used to complement the available component-based models to provide a robust tool for train virtual certification. However, further work is required to overcome the current limitations in the application of the proposed framework, specifically to carry out Monte Carlo simulations to validate the assumption of Gaussian distribution of the prediction uncertainty. In the current work,

all the pantograph components were considered as non-inclined circular cylinders. The actual cross-section geometry, inclination angle, aspect ratio, etc. of each component has to be considered as it will probably increase the obtained uncertainty.

7. REFERENCES

[1] C. Talotte: "Aerodynamic noise: a critical survey," *J. Sound Vib.*, vol. 231, no. 3, pp. 549-62, 2000.

[2] D.J. Thompson: *Railway noise and vibration: mechanisms, modelling and means of control*. 2nd edition. Elsevier; 2024.

[3] C. Mellet, F. Létourneaux, F. Poisson, and C. Talotte: "High speed train noise emission: latest investigation of the aerodynamic/rolling noise contribution," *J. Sound Vib.*, vol. 293, no. 3, pp. 535–546, 2006,

[4] T. Kitagawa and K. Nagakura: "Aerodynamic noise generated by Shinkansen cars," *J. Sound Vib.*, vol. 231, no. 3, pp. 913–924, 2000.

[5] Y. Zhang, J. Zhang, T. Li, and L. Zhang: "Investigation of the aeroacoustic behavior and aerodynamic noise of a high-speed train pantograph.," *Science China Technological Sciences*, vol. 60, pp. 561-575, 2017.

[6] T. Li, D. Qin, W. Zhang and J. Zhang, "Study on the aerodynamic noise characteristics of high-speed pantographs with different strip spacings," *J. Wind. Eng. Ind. Aerodyn.*, vol. 202, p. 104191, 2020.

[7] E. Latorre Iglesias, D.J. Thompson, and M. Smith: "Component-based model to predict aerodynamic noise from high-speed train pantographs," *J. Sound Vib.*, vol. 394, pp. 280-305, 2017.

[8] X. Liu, J. Zhang, J, D.J. Thompson, E. Latorre Iglesias, G. Squicciarini, Z. Hu, M. Toward, and D. Lurcock: "Aerodynamic noise of high-speed train pantographs: Comparisons between field measurements and an updated component-based prediction model". *Appl. Acoust.*, vol. 175, pp. 107791, 2021

[9] N. Furio, M. Starnberg, E. Bongini, D.J. Thompson, U. Orrenius, and N. Cuny: "ACOUTRAIN: virtual certification of acoustic performance for freight and passenger trains," *Energy and Environment*, vol. 1, pp. 491-500, 2016

[10] R. Caminal Barderi, R. Rumpler, A. Curien, A. Cloix, M. Rissmann, A. G. Garcia, I. E. Larrea, and J. Sapena, "Development of Methods for Virtual Exterior Noise Validation Check for updates," *in Noise and Vibration Mitigation for Rail Transportation Systems: Proc. of the 14th International Workshop on Railway Noise*, Shanghai, China, pp. 63-70, Springer Nature, 2024.

[11] E. Bongini, M. Starnberg, R. Cordero, A. Bistagnino, and G. Squicciarini. Uncertainty and variability in acoustic virtual certification process of railway rolling stock. In: Proc. of the 21st International Congress on Sound and Vibration 2014 (ICSV 21), Held 13-17 July 2014, Beijing, China.

[12] E. Latorre Iglesias, J. Xia, M. E. Farooq, A. Bistagnino, and J. Sapena: "Methodology to evaluate the uncertainty of train exterior noise prediction," *Proc. Inst. Mech. Eng., Part C: J. Mech. Eng. Sci.*, vol. 233, no. 18, 6460-6472, 2019

[13] BIPM, IEC, IFCC, ILAC, ISO, IUPAC, IUPAP, and OIML. Evaluation of measurement data — Guide to the expression of uncertainty in measurement. Joint Committee for Guides in Metrology, JCGM 100:2008.

[14] E. Latorre Iglesias, A. L. Gomes Neves, A. Bistagnino, and J. Sapena. Application to Real Cases of a Methodology to Evaluate the Uncertainty of Train Exterior Noise Predictions. *In Noise and Vibration Mitigation for Rail Transportation Systems* pp. 225-233. Springer, Cham, 2021.

[15] E. Latorre Iglesias, D.J. Thompson, and M.G. Smith. "Experimental study of the aerodynamic noise radiated by cylinders with different cross-sections and yaw angles", *J. Sound Vib.*, vol. 361, pp. 108-129, 2016.

[16] Y. Song, F. Duan, F. Wu, Z. Liu, and S. Gao, "Assessment of the current collection quality of pantograph–catenary with contact line height variability in electric railways". *IEEE T. Transp. Electr.*, vol. 8, no. 1, pp. 788-798, 2021.

[17] T. Usuda, M. Ikeda, "Estimation Method of Static Height of Contact Wire by Using Pantograph Contact Force", *Q. Rep. RTRI*, vol. 56, no. 3, pp. 175-180, 2015.

[18] T. Koyama, M. Ikeda, S. Kobayashi, S. K. Tabayashi, and M. Niwakawa, "Measurement of the contact force of the pantograph by image processing technology", *Q. Rep. RTRI*, vol. 55, no. 2, pp. 73-78, 2014.

[19] C. Norberg, "Flow around a circular cylinder: aspects of fluctuating lift", *J. Fluids Struct.* Vol. 15, pp. 459-469, 2001.